Multiple Rabi rotations of trions in InGaAs quantum dots observed by photon echo spectroscopy with spatially shaped laser pulses

S. Grisard [1,*] H. Rose [2] A. V. Trifonov [1] R. Reichhardt [1] D. E. Reiter [3] M. Reichelt [2] C. Schneider [4,5]
M. Kamp [4] S. Höfling [4] M. Bayer [1] T. Meier [2] and I. A. Akimov [1]

[1]*Experimentelle Physik 2, Technische Universität Dortmund, 44221 Dortmund, Germany*
[2]*Paderborn University, Department of Physics & Institute for Photonic Quantum Systems (PhoQS), 33098 Paderborn, Germany*
[3]*Condensed Matter Theory, Technische Universität Dortmund, 44221 Dortmund, Germany*
[4]*Technische Physik, Universität Würzburg, 97074 Würzburg, Germany*
[5]*Institute of Physics, University of Oldenburg, 26129 Oldenburg, Germany*

We study Rabi rotations arising in intensity-dependent photon echoes from an ensemble of self-assembled InGaAs quantum dots. To achieve a uniform distribution of intensities within the excited ensemble, we introduce flattop intensity profiles of picosecond laser pulses. This allows us to overcome the damping of Rabi rotations imposed by the spatial inhomogeneity of Rabi frequencies by a Gaussian laser profile. Using photon echo polarimetry, we distinguish between the coherent optical responses from exciton and trion ensembles. Here, we demonstrate that a photo-induced charging of the quantum dots leads to a significant reduction of the number of neutral quantum dots under resonant excitation with intensive optical pulses with areas exceeding $\pi/2$. The trion ensemble shows robust Rabi rotations when the area of the refocussing pulse is increased up to 5.5π. We analyze the remaining attenuation of Rabi rotations by theoretical modeling of excitation induced dephasing, inhomogeneity of dipole moments, and coupling to acoustic phonons. The latter is identified as the dominating mechanism resulting in a loss of optical coherence during the action of the involved optical pulses.

I. INTRODUCTION

Coherent control over inhomogeneously broadened ensembles of optically addressable qubits is one of the key challenges for the realization of high-capacity storage of quantum light states [1]. Quantum memory protocols in ensembles of qubits are typically based on the photon echo (PE) effect where quantum information stored in an ensemble is reemitted by optically inverting the phase evolution of individual emitters [2]. In this context, excitonic complexes in semiconductor quantum dots (QDs) represent outstanding systems as they typically combine a large ratio between inhomogeneous and homogeneous linewidths with the possibility for subpicosecond optical initialization, which makes them advantageous over atomic vapors [3,4]. As recently demonstrated, the relatively short excitation lifetimes of QDs, that limit potential storage times, can be extended from the picosecond to the nanosecond timescale by transfer between optical and spin coherence [5,6]. However, the use of high optical powers for a complete inversion of the ensemble leads to an irreversible loss of microscopical coherence due to the interaction between the QDs and acoustic phonons [7]. A widely used method to quantify intensity-dependent decoherence mechanisms is the analysis of Rabi rotations as a function of pulse area.

So far, most of the studies on Rabi rotations were performed on single QDs [8–11] because inhomogeneities of

the Rabi frequency often hamper the observation of multiple Rabi cycles. Those inhomogeneities may arise from a spread of dipole moments (resulting from different QD sizes, compositions, etc.) or the coexistence of different excitonic complexes like excitons, trions, or biexcitons within the ensemble [12,13]. Furthermore, coupling to phonons results in a strong dependence on the detuning, which has to be taken into account when an ensemble is considered [14,15]. Finally, the spatial inhomogeneity of the laser intensity profile that covers the QD ensemble induces as major source of dephasing that strongly hinders the experimental observation of Rabi rotations [16].

In this paper, we study Rabi rotations arising in intensity-dependent PEs from an ensemble of self-assembled InGaAs QDs. We manipulate the spatial profiles of picosecond laser pulses to achieve a uniform distribution of intensities within the excited ensemble. This allows us to overcome the damping of Rabi rotations imposed by the spatial inhomogeneity of Rabi frequencies by a Gaussian laser profile while effectively using the available laser power. Using PE polarimetry, we study exciton and trion ensembles independently. Here, we demonstrate that photo-induced charging of the QDs leads to significant reduction of the number of neutral QDs under resonant excitation with intensive optical pulses with areas exceeding $\pi/2$. In this case, most of the QDs in the ensemble are charged and the main contribution to the PE signal is represented by trions that show robust Rabi rotations as a function of the area of the refocussing pulse. We analyze the experimentally observed damping of Rabi rotations by theoretical

*stefan.grisard@tu-dortmund.de

modeling of excitation induced dephasing, inhomogeneity of dipole moments, and phonon-assisted transitions between the dressed states during pulse action.

II. SAMPLE AND METHOD

We study Rabi rotations arising in intensity-dependent PEs on ensembles of (In, Ga)As/GaAs QDs at a temperature of 2 K. The sample consists of a single layer of (In,Ga)As QDs with a density of $1.8 \times 10^9 \, \mathrm{cm}^{-2}$, surrounded by an AlGaAs λ microcavity. The photonic mode of the microcavity is in resonance with the QD ensemble at 1.351 eV as we show in Fig. 1(b) by the photoluminescence spectrum from the sample. The spectrum has a full width at half maximum (FWHM) of 5.9 meV, which results in a quality factor of roughly 230. The same sample was studied before in [17] and [18], where further details can be found. A description of the sample fabrication can be found in [19].

We schematically show the experimental PE setup in Fig. 1(a). Here, two pulses with wavevectors $\mathbf{k}_1$ and $\mathbf{k}_2$ impinge on the sample temporally separated by an adjustable delay of τ_{12}. The first pulse excites a macroscopic polarization that dephases quickly in inhomogeneously broadened systems such as QD ensembles. The second pulse inverts the phase evolution of each excitation independently, which leads to coherent emission in form of a PE at time $2\tau_{12}$ in the phase-matched direction $2\mathbf{k}_2 - \mathbf{k}_1$. We experimentally detect the PE in reflection geometry using the optical heterodyne technique where we capture the interference between the weak signal of interest and a strong reference pulse on a photo diode (PD). By changing the delay τ_{ref} between first and reference pulse, we temporally resolve the photon-echo pulse. Further details about the experimental technique can be found in reference [20]. Figure 1(c) shows the measured temporal cross-correlations between the reference pulse and first, second, and PE pulses where we choose $\tau_{12} = 40 \, \mathrm{ps}$. Note that we normalized the three independently measured peaks to their maximum. The cross-correlations between the reference and first/second pulse both have a FWHM of 5.4 ps reflecting the width of the pulse's amplitude profile $5.4 \, \mathrm{ps}/\sqrt{2} \approx 3.8 \, \mathrm{ps}$. The temporal profile of the PE is given by the Fourier transform of the involved ensemble, hence allowing to extract the inhomogeneous decoherence time T_2^*. In our experiment, however, the spectrum of the laser is more narrow than the cavity mode, as shown in Fig. 1(b). Thus, the PE duration 4.3 ps is mainly determined by the pulse duration. Next to the macroscopic dephasing time T_2^*, our method also allows to extract the homogeneous decoherence time T_2. For that purpose, we capture the maximum value of the PE as a function of the delay τ_{12} by setting the reference time $\tau_{\mathrm{ref}} = 2\tau_{12}$. Results on measurements of T_2 are discussed below.

Rabi oscillations are temporal rotations of the Bloch vector describing the coherent state of a two-level system under action of an optical field. If the optical field is in resonance with the two-level system, the frequency of the Rabi oscillations is given by $\Omega_R = \mu \mathcal{E}/\hbar$, with the dipole moment of the optical transition μ, the light's electric field amplitude $\mathcal{E}$, and the reduced Planck's constant $\hbar$. For laser pulses, this phenomenon yields intensity-dependent Rabi rotations [8,13]. In particular, those intensity-dependent Rabi rotations can be
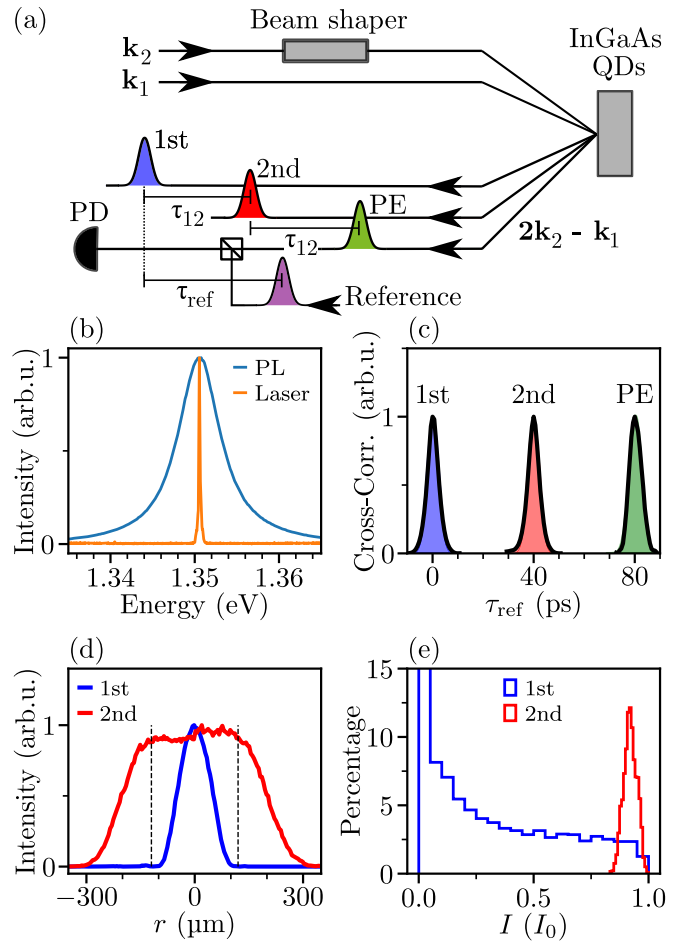

FIG. 1. (a) Experimental scheme for detection of photon echo signals in reflection geometry as described in the main text. (b) Laser spectrum and photoluminescence (PL) spectrum of the studied In-GaAs QD sample placed in a AlGaAs microcavity. The sample spectrum peaks at 1.351 eV and has a FWHM of 5.9 meV, which results in a quality factor of roughly 230. The 0.3 meV narrow spectrum of the laser is tuned to the central wavelength of the PL spectrum. (c) Experimental cross correlations between the reference pulse and all involved pulses in the PE experiment. The pulses have a duration of roughly 3.8 ps. Since the laser spectrum selects a narrow subensemble of QDs, also the PE has a comparable duration to the other pulses. (d) Cross sections of the intensity profiles of first and second beam in the focal plane. The profile of the second beam is manipulated to achieve a flattop distribution in the focus while the first beam remains Gaussian. In this way, we aim to overcome the damping of Rabi rotations by spatial inhomogeneity of Rabi frequencies. (e) Distribution of intensities normalized to the maximum intensity I_0 for the two beams within the radius shown by vertical dashed lines in (d).

observed in a PE experiment as oscillations of the macroscopic polarization when the areas of the first or second pulse are varied in a range strongly exceeding the $\chi^{(3)}$ regime of nonlinear optics [18]. We refer to these oscillations simply as Rabi rotations throughout the article. The dimensionless pulse area A (or integrated Rabi frequency) is defined as $A = \int \Omega_R(t) dt$. Upon changing the areas of first and second pulse (practically, by changing their intensity), the amplitude

P of the PE oscillates according to [21]

$$P \sim \sin(A_1) \sin^2\left(\frac{A_2}{2}\right). \quad (1)$$

Consequently, the PE runs through maxima for $A_1 = (2n + 1)\pi/2$, and $A_2 = (2n + 1)\pi$, respectively, where n is an integer. The simple Eq. (1) strictly holds only for delta-like pulses, while for finite pulses also the temporal shape of the PE can be modulated as a function of pulse area [18]. For the present study, we restricted ourselves to Rabi rotations as a function of the second pulse's area A_2. The area of the first pulse is fixed at $A_1 = \pi/2$, corresponding to the first maximum of the Rabi cycle. The choice of A_2-Rabi rotations is advantageous for the quantitative analysis of the damping of Rabi rotations since sweeping the area of the first pulse also affects the temporal profile of the PE, as demonstrated in [18]. Furthermore, because the sign of the PE amplitude is not affected by the area of the second pulse, A_2 rotations allow us to unambiguously distinguish a fading of Rabi rotations caused by an inhomogeneity of Rabi frequencies within the ensemble from a homogeneous drop of the microscopical polarization.

The distribution of intensities within the finite spot sizes of the laser pulses can introduce a source of fading of Rabi rotations [16,22]. Without modification, all involved laser profiles (first, second, reference) share a Gaussian distribution with the same spot width σ. Consequently, the intensities vary within the spot diameter and the pulse areas in Eq. (1) become dependent on the distance r from the center of the spot. The signal detected by the heterodyne technique may be written in the following form:

$$P(A_1, A_2) \sim \int_0^\infty r \underbrace{e^{-\frac{r^2}{\sigma^2}}}_{\text{Reference}} \sin[A_1(r)] \sin^2\left[\frac{A_2(r)}{2}\right] dr, \quad (2)$$

where we assume radial symmetry of all spatial laser profiles. When both, first and second beam have a Gaussian distribution, i.e., $A_i = A_{i,0} \exp(-r^2/\sigma^2)$ with a maximum pulse area $A_{i,0}$, the Rabi rotations will be strongly damped since the spatial averaging is accompanied by a spread of pulse areas.

Here, we directly compare Rabi rotations with only Gaussian spots with the case that only the first pulse has a Gaussian distribution while the second beam is flat, i.e., $A_2(r) = A_{2,0}$ within the area of spatial overlap between first and second. In this way, the Rabi rotations as a function of $A_{2,0}$, while $A_{1,0}$ is fixed, will not be damped by the effect of spatial averaging. To achieve this condition, we introduce a refractive beam shaper in the path of the second beam [Fig. 1(a)] that converts its Gaussian intensity profile to an Airy disk pattern. By focusing the modified intensity distribution (mathematically, applying the Fourier transformation), we create a flattop intensity distribution as presented in Fig. 1(d). To quantify the difference between the two different intensity profiles, it is useful to consider the distribution of intensities visualized by histograms in Fig. 1(e). For the Gaussian profile, the area within which we can find the same intensities grows with the distance from the center of the spot. Consequently, the intensities are spread over the full intensity range with an increasing trend towards zero. In contrast, the shaped profile narrowly concentrates all intensities around a mean value

close to the maximum intensity I_0. Using the flat intensity profile for the second beam whereas the first beam remains Gaussian, we aim to significantly reduce the damping of Rabi rotations. A simpler approach to achieve the same degree of homogeneity is to use a significantly bigger Gaussian spot for the second beam [12]. However, a similar distribution of intensities as demonstrated in Fig. 1(e), is achieved by using a Gaussian beam with FWHM of roughly 1.2 mm. In this case, however, only 4% of the full intensity contributes to the signal. Especially for the analysis of intensity-dependent damping mechanisms of Rabi rotations, it is of major importance to efficiently use all optical power to reach high values of the pulse area.

III. EXCITONS VS TRIONS

As a first step for the characterization of the QD ensemble, we study the origin of the exciton complexes giving rise to the PE signal. Different complexes such as neutral excitons [Fig. 2(a)] or charged excitons [trions, Fig. 2(b)] can possibly contribute to the signal. We exclude the contribution of biexcitons whose binding energy of roughly 3 meV is significantly larger than the spectral width of the ps-laser pulses [13]. In the context of Rabi rotations, the coexistence of several exciton complexes may cause a source of inhomogeneity of dipole moments that effectively represents a source of damping. However, the polarimetric PE technique allows to carefully analyze the contributions from different exciton complexes and, by appropriate choice of polarizations of the involved laser pulses, to independently address different subensembles. In particular, we apply the PE polarimetry method as introduced in reference [23]. Here, the first pulse is horizontally polarized and the linear polarization angle φ of the second pulse is rotated while the PE amplitude is detected in horizontal polarization. The choice of horizontal polarization for first and reference pulse is arbitrarily chosen since only the relative rotation between the involved polarizations is relevant. The PE amplitude arising from the exciton and trion exhibit a different functional dependence on the angle φ due to the different energy level arrangement and optical transitions, visualized in Figs. 2(a) and 2(b). For the exciton, the PE amplitude is directly affected by the angle φ. For example, as follows from Fig. 2(a), the exciton does not give a response when first and second pulse are linearly cross polarized ($\varphi = \pi/2$). The continuous dependence on the angle φ thus reads as $\cos^2(\varphi)$. For the trion scheme in Fig. 2(b), however, a rotation of the second pulses polarization by the angle φ induces a rotation of the signal's polarization by the angle 2φ, whereas the magnitude of the signal is unaffected. When the signal is detected in horizontal direction, this behavior leads to a $|\cos(2\varphi)|$ dependence. The dependencies for exciton and trion are visualized by polar plots in Figs. 2(c) and 2(d). Note that two configurations play an essential role in distinguishing between excitons and trions. For $\varphi = \pi/2$, only the trion gives a signal, while for $\varphi = \pi/4$ only the exciton contributes. In the latter case, the PE signal is twice smaller due to polarization filtering in the detection. We denote the two configurations as HVH ($\varphi = \pi/2$) and HDH ($\varphi = \pi/4$) in the following, where the letters H, V, or D (horizontal, vertical, diagonal) mark the polarization of the first, second, and reference pulse, respectively.
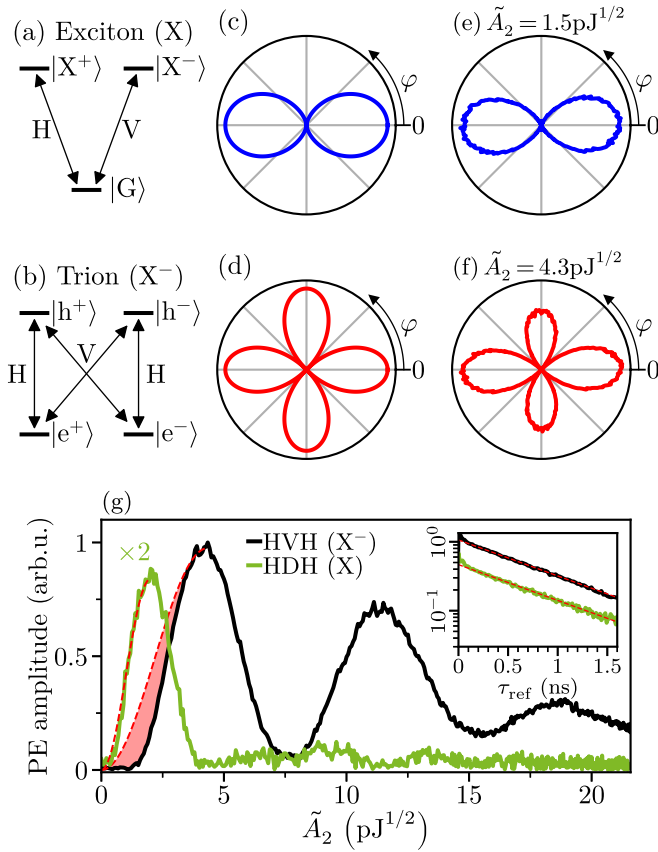
FIG. 2. (a) Schematic picture of the energy level arrangement of an exciton in linear polarization basis, where $|G\rangle$ is the ground state and $|X^{\pm}\rangle = (|X^{\uparrow}\rangle \pm |X^{\downarrow}\rangle)/\sqrt{2}$ are constructed from the spin up/down exciton states $|X^{\uparrow/\downarrow}\rangle$. (b) Trion energy level arrangement, where $|e^{\pm}\rangle = (|e^{\uparrow}\rangle \pm |e^{\downarrow}\rangle)/\sqrt{2}$ denote the ground states with a resident electron and $|h^{\pm}\rangle = (|h^{\uparrow}\rangle \pm |h^{\downarrow}\rangle)/\sqrt{2}$ the excited trion states constructed from the electron (hole) spin up/down states $|e^{\uparrow/\downarrow}\rangle$ ($|h^{\uparrow/\downarrow}\rangle$). The labeled arrows in (a) and (b) mark the allowed optical dipole transitions in the linear polarization basis {H, V}. [(c),(d)] Modeled behavior of exciton and trion within the PE polarimetry experiment, where the linear polarization φ of the second pulse is rotated with respect to the horizontal polarization of the first and reference pulse. [(e),(f)] Measured polarization dependence for two different values of the pulse area of the second pulse as marked in the figure titles. (g) PE amplitude as a function of the pulse area $\tilde{A}_2$ (in units of square root energy per pulse), measured in the polarization configurations HVH and HDH. Dashed lines mark the ideal $\sin^2(A_2/2)$ dependence. Red area highlights the discrepancy between the ideal dependence (dashed line) and the measured data in the configuration HVH in the low power regime. Inset of (g) presents the PE decays measured in the configurations HVH (black) and HDH (green).

In the studied sample, we find that the polarimetric properties are strongly affected by the optical power of the involved pulses, as we demonstrate in Figs. 2(e) and 2(f). The power of the first pulse is fixed, while polar dependencies are measured for two values of the pulse area of the second pulse. To measure the pulse area, we use the square root energy per pulse $\tilde{A}$. For $\tilde{A}_2 = 1.5\,\mathrm{pJ}^{1/2}$ the polar dependence resembles the two-leave rosette of a bare exciton (blue), while for $\tilde{A}_2 = 4.3\,\mathrm{pJ}^{1/2}$ we find a four-leave behavior like for the trion (red).

To study this observation in detail, we continuously measure the intensity dependence of the PE amplitude in the configurations HVH (trion) and HDH (exciton), presented in Fig. 2(g). In the HVH configuration, we find a pronounced Rabi rotations of the ensemble featuring three local maxima that we can associate with pulse areas of the second pulse $A_2 = \pi$, 3π, 5π and two local minima for $A_2 = 2\pi$, 4π, see Eq. (1). In contrast, the Rabi rotations captured in the configuration HDH appears strongly damped, only one maximum can be observed. Furthermore, the first maximum of the trion appears shifted towards higher optical powers by a factor of 2.2 with respect to the exciton. A shift of the maxima could be caused by different dipole moments of exciton and trion. However, the dominant mechanisms for the different damping of the Rabi rotations of exciton and trions is revealed by considering the intensity dependence of the signal strength for the trion in the range up to the first maximum. For the exciton, the signal follows a $\sin^2(A_2/2)$ dependence as predicted by Eq. (1), highlighted by the red dashed line in Fig. 2(g). For the trion, however, we can observe a strong deviation that we highlight by the red area in Fig. 2(g). The signal in HVH rather follows a polynomial function of higher degree in the low power range indicating that another power-dependent contribution leads to an increase of the trion signal. We associate this finding with a photo-charging of the QDs [24,25]. Increasing the optical power thus induces a rising of the number of singly charged QDs. Accordingly, the number of neutral excitons is decreased, which explains the strong damping of the photon-echo signal measured in the configuration HDH. We note that the process of QD discharging acts on the timescale of microseconds and is thus significantly slower than the decoherence times of excitons and trions [26]. Therefore, it does not influence the temporal dynamics of PEs and their decay. However, it changes the ratio between the number of excitons and trions contributing to the signal. If necessary, the same charging state of the QDs can be initialized in a controlled manner also by nonresonant illumination of the sample.

As a final remark to the polarimetry studies, we provide experimental values for the homogeneous linewidth associated with excitons and trions. In the inset of Fig. 2(g), we show the decays of the PE amplitude measured in HDH and HVH. For both resonances, we extract $T_2 = 0.83\,\mathrm{ns}$ corresponding to a linewidth of $\Gamma = 2\hbar/T_2 = 1.6\,\mu\mathrm{eV}$. For the discussion of damping mechanisms of the Rabi rotations, we restrict ourselves to the polarization configuration HVH where we exclusively detect charged QDs.

IV. DISCUSSION OF DAMPING MECHANISMS

We aim to gain a deeper understanding into the underlying mechanisms that evoke the loss of macroscopic coherence in intensity-dependent PE experiments. First, we discuss the possible conclusions that can be drawn from a detailed consideration of the experimental data. Afterwards, we introduce a theoretical modeling procedure taking into account a variety of damping mechanisms that are either inherent to every single QD or are associated with the inhomogeneity of the ensemble. The comparison of model and experiment allows to quantify the contribution of each decoherence channel. We want to stress that the usage of a flattop intensity profile
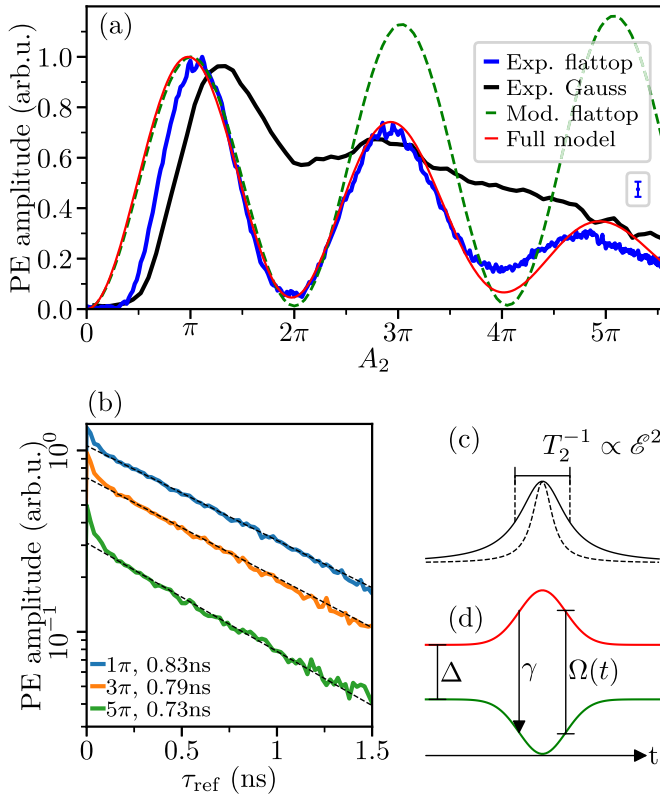
FIG. 3. (a) Experimentally observed Rabi rotations as a function of the second pulse's area A_2 for Gaussian and flattop intensity profiles. Red and green curve show results of our modeling procedure as described in the text. Note that the maximum uncertainty associated with the measured values of the PE amplitude amounts to roughly 3×10^{-2}, which we visualize by the error bar shown below the legend in (a). (b) Decays of the PE amplitude for $A_2 = \pi$, 3π, 5π (local extrema of Rabi cycle), measured using the flattop intensity profile for second beam. Time values in the legend are results for the decoherence time T_2 extracted by fits (dashed lines). All experimental data shown in (a) and (b) where recorded in the polarization configuration HVH. (c) Schematic illustration of excitation induced dephasing, that describes a broadening of the homogeneous linewidth, i.e., a shortening of T_2 with increasing excitation power $\sim \mathcal{E}^2$. (d) Schematic illustration of the phonon model discussed in the main text.

is key to uncover internal sources of damping, which we demonstrate in Fig. 3(a). Here, we compare the Rabi rotations measured using a flattop intensity profile (blue) with those measured with only Gaussian laser spots (black). Note that in the case of Gaussian spots, the Rabi cycle is strongly faded by the inhomogeneity of Rabi frequencies. The manipulation of the laser beam profile by means of a refractive beam profiler thus allows to strongly reduce the effect of spatial averaging. As we will show below, the effect of spatial inhomogeneity is negligible using the manipulated flattop profile as characterized in Fig. 1(d). We thus discuss further possible contributions to the damping mechanisms.

The measured Rabi rotations in Fig. 3(a) feature a strong drop of the contrast between the local maxima and minima with increasing pulse area. The contrast between the π maximum and the 2π minimum is roughly 90% whereas the contrast between the 4π minimum and 5π maximum

amounts to only 30%. This drop can be associated with an inhomogeneous broadening of dipole moments, which leads to a complete loss of contrast with increasing pulse area. Since the PE signal depends on $\sin^2(A_2/2)$, the overall PE signal will reach a constant value of 50% of the maximum value. In our data, we can observe that the PE signal significantly drops below the value of 50% as the PE amplitude at $A_2 = 5\pi$ drops to roughly 30% of its maximum value. We therefore conclude that despite the damping mechanisms that are associated with the ensemble, we have to take into account decoherence effects that are inherent to a single QD.

A well-known intrinsic contribution to the damping of Rabi rotations is excitation induced dephasing (EID) that describes a broadening of the homogeneous spectral linewidth $\Gamma \sim T_2^{-1}$ with increasing excitation power, as we sketch in Fig. 3(c). Possible contributions to EID such as the coupling to phonons or wetting layer states were intensively studied in several publications [27–30]. Here, we only aim to quantify the contribution of EID by measuring the decoherence time T_2 as a function of excitation power. In Fig. 3(b) we measured the decay of the PE amplitude for $A_2 = \pi$, 3π, 5π. We notice that the decrease of the PE amplitude goes along with a gradual drop of T_2 from 0.83 ns at $A_2 = \pi$ over 0.79 ns at $A_2 = 3\pi$ to 0.73 ns at $A_2 = 5\pi$. We can conclude that EID is present in the studied sample and the accelerated decay directly damps the PE with a factor of $\exp[-\tau_{\mathrm{ref}}/T_2(A_2)]$, where $T_2(A_2)$ is the pulse-area-dependent decoherence time. However, since we measure the Rabi rotations for a relatively short delay of $\tau_{\mathrm{ref}} = 80$ ps, the contribution of EID on the drop of amplitude is negligible as emerges from the estimation $e^{-\frac{80\mathrm{ps}}{T_2(5\pi)}}/e^{-\frac{80\mathrm{ps}}{T_2(\pi)}} \approx 99\%$. Instead, the strong decrease of the PE amplitude can solely be explained by a drop of initial value of signal with increase of pulse area, which is in agreement with Fig. 3(b). We therefore expand our consideration of decoherence beyond the broadening of the homogeneous linewidth and describe our full modeling procedure in the following.

We consider phonon-assisted relaxation processes during the action of the laser pulses that occur due to the optical dressing of the involved QD states. The importance of the effect has been demonstrated recently in phonon-assisted state preparation schemes of QDs [15] or in the context of single photon-sources [31]. The idea of the process is illustrated in Fig. 3(d) and will be described in the following. The trion ensemble is considered as an ensemble of two-level systems (TLS) composed of the ground state $|1\rangle$ and the excited state $|2\rangle$, which is justified in the absence of a magnetic field. The density matrix ρ of a single TLS is a 2×2 matrix for a given basis. We define $\rho_{12} = \langle 1|\rho|2\rangle$ as microscopic polarization and $\rho_{22} = \langle 2|\rho|2\rangle$ as occupation of the excited state. Computing the dynamic of the density matrix elements ρ_{12} and ρ_{22} in the bare-state (BS) basis leads to the optical Bloch equations (OBEs) [32]. The energy separation between the two states is given by the detuning Δ in rotating wave approximation. Upon interaction with a light field, the total Hamiltonian is diagonal in the dressed state (DS) basis with a modified energy splitting given by the generalized Rabi frequency $\Omega = \sqrt{\Omega_R^2 + \Delta^2}$. A transition to the DS basis is advantageous when treating the interaction with longitudinal acoustic phonons, since their effect can be modeled

approximately by introducing a loss rate γ in the equations of motion [14,33]. The dynamics of the density matrix elements in the DS basis is given by [14]

$$\frac{\partial}{\partial t}\rho_{12}^{\mathrm{DS}} = -i\Omega\rho_{12}^{\mathrm{DS}} - \frac{\gamma}{2}\rho_{12}^{\mathrm{DS}}, \tag{3}$$

$$\frac{\partial}{\partial t}\rho_{22}^{\mathrm{DS}} = -\gamma\rho_{22}^{\mathrm{DS}}. \tag{4}$$

The phononic loss rate γ is modeled as [14]

$$\gamma = \frac{\pi}{2}\left(\frac{\Omega_R}{\Omega}\right)^2 J(\Omega), \tag{5}$$

$$J(\omega) = A\omega^3 \exp\left(-\frac{\omega^2}{\omega_c^2}\right), \tag{6}$$

where $J(\omega)$ is the phonon spectral density with the cut-off frequency ω_c and the amplitude A of the coupling strength. The phonon spectral density represents a measure for the efficiency of coupling between carriers and acoustical phonons for a given Rabi frequency Ω. Equation (6) assumes a spherical shape of the QDs, which may be a strong simplification for the shape of the studied QDs. However, by appropriate choice of the parameters A and ω_c, an arbitrary geometry of QDs may be sufficiently well approximated [34]. Therefore, we use A and ω_c as fitting parameters of our modeling procedure.

Because in the considered approach the dephasing and relaxation induced by the phonons are only present during the excitation with an optical field, the free evolution of the system, temporally between the optical pulses, can be computed in the BS basis by OBEs in the rotating-wave approximation [32]

$$\frac{\partial}{\partial t}\rho_{12}^{\mathrm{BS}} = i\Delta\rho_{12}^{\mathrm{BS}}, \tag{7}$$

$$\frac{\partial}{\partial t}\rho_{22}^{\mathrm{BS}} = 0. \tag{8}$$

The transformation between these bases is given by $\rho^{\mathrm{DS}} = V^{-1}\rho^{\mathrm{BS}}V$, where the matrix V reads [14]

$$V = \frac{1}{\sqrt{2\Omega}}\begin{bmatrix} \sqrt{\Omega-\Delta} & \sqrt{\Omega+\Delta} \\ \sqrt{\Omega+\Delta} & -\sqrt{\Omega-\Delta} \end{bmatrix}. \tag{9}$$

Note that this transformation is defined for a fixed Rabi frequency Ω_R. To describe pulses with Gaussian temporal shape and duration of 3.8 ps that are used in the experiment, we approximate the time-dependent Rabi frequency $\Omega_R(t)$ by a step-like function with fixed values for finite temporal intervals.

To expand the described approach for an ensemble of TLS, we introduce three indices in the equations of motion

$$\frac{\partial}{\partial t}\left[\rho_{12}^{\mathrm{DS}}\right]_{\mathrm{i,d,s}} = -i\Omega_{\mathrm{i,d,s}}\left[\rho_{12}^{\mathrm{DS}}\right]_{\mathrm{i,d,s}} - \frac{\gamma_{\mathrm{i,d,s}}}{2}\left[\rho_{12}^{\mathrm{DS}}\right]_{\mathrm{i,d,s}}, \tag{10}$$

$$\frac{\partial}{\partial t}\left[\rho_{22}^{\mathrm{DS}}\right]_{\mathrm{i,d,s}} = -\gamma_{\mathrm{i,d,s}}\left[\rho_{22}^{\mathrm{DS}}\right]_{\mathrm{i,d,s}}, \tag{11}$$

$$\frac{\partial}{\partial t}\left[\rho_{12}^{\mathrm{BS}}\right]_{\mathrm{i,d,s}} = i\Delta_{\mathrm{i}}\left[\rho_{12}^{\mathrm{BS}}\right]_{\mathrm{i,d,s}}, \tag{12}$$

$$\frac{\partial}{\partial t}\left[\rho_{22}^{\mathrm{BS}}\right]_{\mathrm{i,d,s}} = 0. \tag{13}$$

In that way, we are able to account for inhomogeneous broadening of the QD ensemble (index i), randomly distributed dipole matrix elements (index d), and the spatial profile of the electric field (index s). The modeling procedure relies on numerical integration of Eqs. (10)–(13). Subsequently, the ensemble averages over the three indices i, d, s are performed as described in the following. First, the macroscopic polarization is obtained by summation over the inhomogeneous broadening, given by a weight function L,

$$P_{\mathrm{d,s}}(t) = \mu_{\mathrm{d}}\sum_{\mathrm{i}}L(\Delta_{\mathrm{i}})p_{\mathrm{i,d,s}}(t) \tag{14}$$

For all calculations we assume a Lorentzian distribution of detunings $L(\Delta_{\mathrm{i}})$ with a FWHM of 5.9 meV as extracted from photoluminescence measurements, Fig. 1(b). Second, for the spread of dipole moments (index d), we assume a Gaussian distribution $\tilde{G}(\mu_{\mathrm{d}})$ whose width is a free fitting parameter. The ensemble average is given by

$$P_{\mathrm{s}}(t) = \sum_{\mathrm{d}}\tilde{G}(\mu_{\mathrm{d}})P_{\mathrm{d,s}}. \tag{15}$$

Finally, the summation over the spatial profiles (index s) is carried out by taking into account the spatial profile of the reference beam $E_{\mathrm{s}}^{\mathrm{ref}}$, which equals the Gaussian spatial profile of the first pulse

$$P(t) = 2\pi\sum_{\mathrm{s}}r_{\mathrm{s}}\Delta r E_{\mathrm{s}}^{\mathrm{ref}}P_{\mathrm{s}}(t), \tag{16}$$

where we assumed radial symmetry. Δr is the stepwidth for the discretization of the radial distance from the center of the spots r. The final signal is obtained by convoluting $P(t)$ with the reference pulse, which is assumed to have the same properties as the first pulse.

The differential equations are solved with the fourth-order Runge-Kutta method with a step-width of $d\tau = 0.02$ ps. The pulses are modeled as Gaussian function with a FWHM of 3.8 ps, discretized into 501 steps, which are sampled within an interval of 20 ps centered around the pulse. For the inhomogeneous broadening, $N = 800$ TLS were taken into account covering the detuning range from -15 meV to $+15$ meV. The decoherence time T_2 is included a posteriori to the simulation of the sections at $\tau_{\mathrm{ref}} = 2\tau_{12}$, by multiplying with $\exp(-\frac{2\tau_{12}}{T_2(A_2)})$, where $T_2(A_2)$ is a function that is obtained from a linear fit of the experimentally measured T_2 values, Fig. 3(b).

The described modeling procedure allows us to study individual decoherence mechanisms and to quantify their contribution to the overall damping. First, we use our model to specify the spatial homogeneity of the flattop intensity profile. Figure 3(a) shows the modeled Rabi rotations where solely the experimental intensity distribution of the flattop laser profile is taken into account (green dashed line). No damping is observable within the measured intensity range. Therefore, we conclude that our experimental method allows to overcome the effect of spatial averaging. Note that the modeled PE has a lower amplitude for $A_2 = \pi$ than for $A_2 = 3\pi$. This deviation from the simplified $\sin^2(A_2/2)$ dependence [Eq. (1)] arises from the finite duration of the optical pulses as discussed above.

Finally, we take into account all discussed damping mechanisms and optimize the free parameters of our model to

fit the measured Rabi rotations. We find the best agreement between model and experiment for $A = 0.012(1)\,\mathrm{ps}^2$, $\omega_c = 3.6(1)\,\mathrm{THz}$, and a dipole inhomogeneity of 21(2)% (FWHM), which are in reasonable agreement with results obtained from similar QD samples [13–15]. The resulting Rabi rotation is plotted in Fig. 3(a) together with the experimental data. Note that the modeling procedure does not take into account the photo charging effect that we discussed in the previous section. Therefore, the modeled curve deviates from the experimental data in the range $A_2 \lesssim \pi$. Excellent agreement between model and experiment is found in the range $\pi \lesssim A_2 \lesssim 3.5\pi$, whereas the contrast of the measured oscillations is less pronounced for $A_2 \gtrsim 3.5\pi$ as described by our model. Nevertheless, the comparison between the experimental and modeled Rabi rotations in combination with the study of EID allows us to conclude that the coupling to acoustic phonons is the dominant mechanism for the loss of optical coherence inherent to a single dot. For the used pulse durations of 3.8 ps, the largest pulse areas in our experiment $\sim 5\pi$ feature a mean Rabi frequency of roughly 4.1 THz, which is close to the maximum of the phonon spectral density (6) with the found parameters. Consequently, the loss of coherence acts very efficient in the regime of large pulse areas. By use of longer ($\sim 50\,\mathrm{ps}$) or shorter ($\sim 100\,\mathrm{fs}$) pulses, the coupling to phonons could be strongly reduced [35].

V. CONCLUSIONS

We experimentally observed Rabi rotations in intensity-dependent PEs from an ensemble of InGaAs QDs. Through application of the PE polarimetry method, we independently considered resonant excitation of excitons and trions and the resulting PE signals from these complexes. In the studied sample, the increase of optical power induces a rising number of charged QDs and decrease of neutral QDs due to photo-induced charging. Already for moderate excitation powers with area of π, the majority of QDs are charged which allows to limit the consideration of one subensemble where the coherent response stems from an ensemble of trions. Rabi rotations on the trion population serve further as a tool to study intensity-dependent damping mechanisms that are associated with single dots and the ensemble. We successfully implemented a refractive beam shaper to achieve a uniform distribution of Rabi frequencies. Thereby, we demonstrated Rabi rotations up to roughly 5.5π allowing to discuss in detail different contributions to the damping. We found that the dominating source of damping inherent to a single dot is the efficient interaction with acoustic phonons. This interaction, however, is low for pulse areas up to π. Hence, more complex pulse arrangements including more than two pulses with areas up to π as needed for quantum memory applications may be realized with high efficiency. Furthermore, the interaction with phonons for a given pulse area can be strongly reduced by extending or shortening the optical pulses.

The data that support the findings of this study are available from the corresponding author upon reasonable request.

[1] A. I. Lvovsky, B. C. Sanders, and W. Tittel, Optical quantum memory, Nat. Photonics **3**, 706 (2009).

[2] W. Tittel, M. Afzelius, T. Chaneliére, R. Cone, S. Kröll, S. Moiseev, and M. Sellars, Photon-echo quantum memory in solid state systems, Laser Photonics Rev. **4**, 244 (2009).

[3] D. F. Phillips, A. Fleischhauer, A. Mair, R. L. Walsworth, and M. D. Lukin, Storage of Light in Atomic Vapor, Phys. Rev. Lett. **86**, 783 (2001).

[4] L.-M. Duan, M. D. Lukin, J. I. Cirac, and P. Zoller, Long-distance quantum communication with atomic ensembles and linear optics, Nature (London) **414**, 413 (2001).

[5] L. Langer, S. V. Poltavtsev, I. A. Yugova, M. Salewski, D. R. Yakovlev, G. Karczewski, T. Wojtowicz, I. A. Akimov, and M. Bayer, Access to long-term optical memories using photon echoes retrieved from semiconductor spins, Nat. Photonics **8**, 851 (2014).

[6] A. N. Kosarev, A. V. Trifonov, I. A. Yugova, I. I. Yanibekov, S. V. Poltavtsev, A. N. Kamenskii, S. E. Scholz, C. Sgroi, A. Ludwig, A. D. Wieck *et al.*, Extending the time of coherent optical response in ensemble of singly-charged InGaAs quantum dots, arXiv:2201.09383.

[7] E. A. Muljarov and R. Zimmermann, Dephasing in Quantum Dots: Quadratic Coupling to Acoustic Phonons, Phys. Rev. Lett. **93**, 237401 (2004).

[8] T. H. Stievater, X. Li, D. G. Steel, D. Gammon, D. S. Katzer, D. Park, C. Piermarocchi, and L. J. Sham, Rabi Oscillations of Excitons in Single Quantum Dots, Phys. Rev. Lett. **87**, 133603 (2001).

[9] D. Wigger, C. Schneider, S. Gerhardt, M. Kamp, S. Höfling, T. Kuhn, and J. Kasprzak, Rabi oscillations of a quantum dot exciton coupled to acoustic phonons: Coherence and population readout, Optica **5**, 1442 (2018).

[10] L. Monniello, C. Tonin, R. Hostein, A. Lemaitre, A. Martinez, V. Voliotis, and R. Grousson, Excitation-Induced Dephasing in a Resonantly Driven InAs/GaAs Quantum Dot, Phys. Rev. Lett. **111**, 026403 (2013).

[11] A. Zrenner, E. Beham, S. Stufler, F. Findeis, M. Bichler, and G. Abstreiter, Coherent properties of a two-level system based on a quantum-dot photodiode, Nature (London) **418**, 612 (2002).

[12] T. Suzuki, R. Singh, M. Bayer, A. Ludwig, A. D. Wieck, and S. T. Cundiff, Detuning dependence of Rabi oscillations in an InAs self-assembled quantum dot ensemble, Phys. Rev. B **97**, 161301(R) (2018).

[13] P. Borri, W. Langbein, S. Schneider, U. Woggon, R. L. Sellin, D. Ouyang, and D. Bimberg, Rabi oscillations in the excitonic ground-state transition of InGaAs quantum dots, Phys. Rev. B **66**, 081306(R) (2002).

[14] M. R. Klaßen and D. E. Reiter, Optical signals to monitor the dynamics of phonon-modified Rabi oscillations in a quantum dot, Ann. Phys. **533**, 2100086 (2021).

[15] J. H. Quilter, A. Brash, F. Liu, M. Glässl, A. M. Barth, V. M. Axt, A. J. Ramsay, M. S. Skolnick, and A. M. Fox, Phonon-Assisted Population Inversion of a Single InGaAs/GaAs Quantum Dot by Pulsed Laser Excitation, Phys. Rev. Lett. **114**, 137401 (2015).

[16] S. V. Poltavtsev, M. Reichelt, I. A. Akimov, G. Karczewski, M. Wiater, T. Wojtowicz, D. R. Yakovlev, T. Meier, and M. Bayer, Damping of Rabi oscillations in intensity-dependent photon echoes from exciton complexes in a CdTe/(Cd,Mg)Te single quantum well, Phys. Rev. B **96**, 075306 (2017).

[17] A. N. Kosarev, H. Rose, S. V. Poltavtsev, M. Reichelt, C. Schneider, M. Kamp, S. Höfling, M. Bayer, T. Meier, and I. A. Akimov, Accurate photon echo timing by optical freezing of exciton dephasing and rephasing in quantum dots, Commun. Phys. **3**, 228 (2020).

[18] S. V. Poltavtsev, M. Salewski, Y. V. Kapitonov, I. A. Yugova, I. A. Akimov, C. Schneider, M. Kamp, S. Höfling, D. R. Yakovlev, A. V. Kavokin, and M. Bayer, Photon echo transients from an inhomogeneous ensemble of semiconductor quantum dots, Phys. Rev. B **93**, 121304(R) (2016).

[19] S. Maier, P. Gold, A. Forchel, N. Gregersen, J. Mørk, S. Höfling, C. Schneider, and M. Kamp, Bright single photon source based on self-aligned quantum dot–cavity systems, Opt. Express **22**, 8136 (2014).

[20] S. V. Poltavtsev, I. A. Yugova, I. A. Akimov, D. R. Yakovlev, and M. Bayer, Photon echo from localized excitons in semiconductor nanostructures, Phys. Solid State **60**, 1635 (2018).

[21] P. R. Berman and V. S. Malinovsky, *Principles of Laser Spectroscopy and Quantum Optics* (Princeton University Press, Princeton, 2010).

[22] M. Kujiraoka, J. Ishi-Hayase, K. Akahane, N. Yamamoto, K. Ema, and M. Sasaki, Optical Rabi oscillations in a quantum dot ensemble, Appl. Phys. Express **3**, 092801 (2010).

[23] S. V. Poltavtsev, Y. V. Kapitonov, I. A. Yugova, I. A. Akimov, D. R. Yakovlev, G. Karczewski, M. Wiater, T. Wojtowicz, and M. Bayer, Polarimetry of photon echo on charged and neutral excitons in semiconductor quantum wells, Sci. Rep. **9**, 5666 (2019).

[24] L. Dusanowski, C. Nawrath, S. L. Portalupi, M. Jetter, T. Huber, S. Klembt, P. Michler, and S. Höfling, Optical charge injection and coherent control of a quantum-dot spin-qubit emitting at telecom wavelengths, Nat. Commun. **13**, 748 (2022).

[25] M. Johnsson, D. R. Góngora, J. P. Martinez-Pastor, T. Volz, L. Seravalli, G. Trevisi, P. Frigeri, and G. Muñoz-Matutano, Ultrafast Carrier Redistribution in Single InAs Quantum Dots Mediated by Wetting-Layer Dynamics, Phys. Rev. Appl. **11**, 054043 (2019).

[26] A. Kurzmann, A. Ludwig, A. D. Wieck, A. Lorke, and M. Geller, Auger recombination in self-assembled quantum dots: Quenching and broadening of the charged exciton transition, Nano Lett. **16**, 3367 (2016).

[27] P. Borri, W. Langbein, U. Woggon, V. Stavarache, D. Reuter, and A. D. Wieck, Exciton dephasing via phonon interactions in InAs quantum dots: Dependence on quantum confinement, Phys. Rev. B **71**, 115328 (2005).

[28] S. Lüker and D. E. Reiter, A review on optical excitation of semiconductor quantum dots under the influence of phonons, Semicond. Sci. Technol. **34**, 063002 (2019).

[29] A. J. Ramsay, A. V. Gopal, E. M. Gauger, A. Nazir, B. W. Lovett, A. M. Fox, and M. S. Skolnick, Damping of Exciton Rabi Rotations by Acoustic Phonons in Optically Excited InGaAs/GaAs Quantum Dots, Phys. Rev. Lett. **104**, 017402 (2010).

[30] H. C. Schneider, W. W. Chow, and S. W. Koch, Excitation-induced dephasing in semiconductor quantum dots, Phys. Rev. B **70**, 235308 (2004).

[31] S. E. Thomas, M. Billard, N. Coste, S. C. Wein, Priya, H. Ollivier, O. Krebs, L. Tazaïrt, A. Harouri, A. Lemaitre, I. Sagnes, C. Anton, L. Lanco, N. Somaschi, J. C. Loredo, and P. Senellart, Bright Polarized Single-Photon Source Based on a Linear Dipole, Phys. Rev. Lett. **126**, 233601 (2021).

[32] L. Allen and J. H. Eberly, *Optical Resonance and Two-Level Atoms* (John Wiley & Sons, Nashville, TN, 1975).

[33] D. E. Reiter, Time-resolved pump-probe signals of a continuously driven quantum dot affected by phonons, Phys. Rev. B **95**, 125308 (2017).

[34] S. Lüker, T. Kuhn, and D. E. Reiter, Phonon impact on optical control schemes of quantum dots: Role of quantum dot geometry and symmetry, Phys. Rev. B **96**, 245306 (2017).

[35] P. Machnikowski and L. Jacak, Resonant nature of phonon-induced damping of Rabi oscillations in quantum dots, Phys. Rev. B **69**, 193302 (2004).